Cryoegg: development and field trials of a wireless subglacial probe for deep, fast-moving ice

Michael Prior-Jones[1], Elizabeth Bagshaw[1], Jonathan Lees[2], Lindsay Clare[3], Stephen Burrow[3], Mauro A Werder[4], Nanna B. Karlsson[5], Dorthe Dahl-Jensen[6,7], Thomas R. Chudley[8], Poul Christoffersen[8], Jemma Wadham[9], Samuel H Doyle[10], Bryn Hubbard[10]

[1] School of Earth and Ocean Sciences, Cardiff University, Cardiff, UK (prior-jonesm@cardiff.ac.uk; bagshawe@cardiff.ac.uk)
[2] School of Engineering, Cardiff University, Cardiff, UK
[3] Department of Aerospace Engineering, University of Bristol, Bristol, UK
[4] Laboratory of Hydraulics, Hydrology and Glaciology, ETH Zürich, Zürich, Switzerland
[5] Geological Survey of Denmark and Greenland, Copenhagen, Denmark
[6] Niels Bohr Institute, University of Copenhagen, Copenhagen, Denmark
[7] Center for Earth Observation Science, University of Manitoba, Winnipeg, Canada
[8] Scott Polar Research Institute, University of Cambridge, Cambridge, UK
[9] School of Geographical Sciences, University of Bristol, Bristol, UK
[10] Department of Geography and Earth Sciences, Aberystwyth University, Aberystwyth, UK

ABSTRACT

Subglacial hydrological systems require innovative technological solutions to access and observe. Wireless sensor platforms can be used to collect and return data, but their performance in deep and fast-moving ice requires quantification. We report experimental results from Cryoegg: a spherical probe that can be deployed into a borehole or moulin and transit through the subglacial hydrological system. The probe measures temperature, pressure and electrical conductivity in-situ and returns all data wirelessly via a radio link. We demonstrate Cryoegg's utility in studying englacial channels and moulins, including in-situ salt dilution gauging. Cryoegg uses very high frequency (VHF) radio to transmit data to a surface receiving array through up to 1.3 km of cold ice - a significant improvement on the previous design. The wireless transmission uses Wireless M-Bus on 169 MHz; we present a simple radio link budget model for its performance in cold ice and experimentally confirm its validity. Cryoegg has also been tested successfully in temperate ice. The battery capacity allows measurements to be made every two hours for more than a year. Future iterations of the radio system will enable Cryoegg to transmit data through up to 2.5 km of ice.

INTRODUCTION

The presence and behaviour of water in the subglacial environment governs the response of ice to climate warming. Meltwater generated on the surface makes its way to the bed via networks of moulins, cracks and crevasses (Chu, 2014; Flowers, 2018). Once at the bed, it flows to the ice margins either through a subglacial drainage network consisting of inefficient linked cavities (Iken and Bindschadler, 1986; Walder, 1986; Kamb, 1987), efficient channels carved into rock, ice or the sediment below (Röthlisberger, 1972; Nye, 1976; Clarke, 1987; Ng, 2000), or a combination of both (Hoffman and others, 2016). The configuration of the drainage network determines the subglacial water pressure and how much of the ice-bed interface is in contact with liquid water. Contact promotes sliding (Kamb, 1970; Iken, 1981; Schoof, 2010), which in turn can cause ice to accelerate downstream. In recent years, the relationship between meltwater supply and ice acceleration has been reevaluated in light of observations from the margins of the Greenland Ice Sheet that demonstrate a seasonal evolution of subglacial drainage systems (Chandler and others, 2013; Tedstone and others, 2015) commonly observed in Alpine systems (Nienow and others, 2005). Early in the melt season, an increased flux of meltwater is routed to the bed and the low capacity, inefficiently linked cavity system is forced to expand, forming efficient channels that can transport substantial volumes of water. This reduces the area of the bed in contact with water, and potentially, regulates the flow of ice (Sole and others, 2011; Tedstone and others, 2015; Nienow and others, 2017; Flowers, 2018). The defining feature of these different drainage configurations is the water pressure: channelised systems operate at lower pressure than linked cavities, thus measurement of the subglacial water pressure can be used to determine the likely structure of the drainage system, and hence the acceleration response of the ice to increased surface melt inputs.

In addition to water pressure, other parameters may provide clues as to the structure of the drainage system, but distinction between drainage system types is challenging. Temperature can be used to assess whether the bed is at the pressure melting point, and the residence time of water in the system can be used, in conjunction with pressure, to assess how efficiently the meltwater transits the system. Long residence times are common in linked cavity systems, which results in prolonged contact between meltwater and subglacial sediment (Tranter and others, 2002). This promotes chemical weathering and changes the composition of the meltwater, so meltwater chemistry is a good indicator of drainage system structure. Chemical composition is challenging to assess in situ, but a measurement of the total dissolved solids can be easily obtained via a measurement of electrical conductivity (Hubbard and others, 1995).

These three parameters (pressure (P), temperature (T) and electrical conductivity (EC)) are relatively easy to measure via electronic sensors and can thus be combined to provide information on subglacial drainage that could not be detected from the surface. Measuring these parameters subglacially is, however, extremely challenging, particularly beneath thick, fast flowing ice. Yet it is these fast-flowing sectors that govern the response of large ice masses to climate warming, since they transfer significant volumes of ice to the ocean (Pritchard and others, 2009; Broeke and others, 2016). Drilling boreholes through a glacier to access subglacial hydrological channels is logistically demanding and disturbs the system that is under study. Once boreholes are drilled, implanting cabled sensors is possible, but ice motion causes cables to flex and eventually break (Iken and others, 1993; Doyle and others, 2018). In fast-flowing ice, data capture is thus limited to days or weeks. An alternative method is therefore required that can capture these relatively simple electrical measurements and return them to the surface without requiring a physical connection. A wireless radio frequency (RF) system is ideal and there is a long history of the use of RF propagation through ice (see Plewes and Hubbard, 2016 for a review).

Here, we present trials of Cryoegg, a wireless sensor platform for use in deep ice. The use of a radio link for subglacial telemetry has been proven by the work of the Glacsweb programme (Martinez and others, 2004; Hart and others, 2019) and the WiSe project (Smeets and others, 2012). Previous work (Bagshaw and others, 2014) showed that a 'Cryoegg' concept was feasible, namely a spherical sensor platform containing all sensor, radio and datalogger components that could fit in a standard borehole and travel through subglacial meltwater pathways: the electronics could be made sufficiently compact, and that the radio link worked through up to 500m of ice. However, the radio link design chosen proved unsuitable for performance in very deep ice, so design improvements were required. In this paper we describe the redesign of Cryoegg to give enhanced radio link performance and show the outcomes of field trials at sites in Greenland and the Swiss Alps.

In order to measure subglacial hydrological properties in deep polar ice, the enhanced Cryoegg had to meet or exceed the following engineering constraints:

- An outer diameter of 120 mm or less, to fit into a standard ice core borehole
- A radio link capable of reaching the surface through 2,500 m of ice, the mean bed depth in central Greenland (Morlighem and others, 2017)
- Survive and measure water pressure of up to 250 bar (equivalent to a water column of 2,500 m)
- Measure temperature, typically in the range from -30 to 0 °C
- Measure EC, typically in the range from 2 µS cm^{-1} to 250 µS cm^{-1}
- A battery life capable of sustaining one measurement every 12 hours for a period of one year

RADIO LINK DESIGN

The success of the instrument depends principally on the performance of the radio link. The 2012 design (Bagshaw and others, 2014) used a simple frequency shift keying (FSK) transmitter operating on 151 MHz and demonstrated a maximum range of 500 m in wet ice. To achieve a greater range, we investigated alternative frequencies and transmission schemes. The power of a radio wave propagating in "free space" (e.g. in air or vacuum) reduces according to an inverse square law with distance - known as "geometric attenuation". When the propagating wave reaches a receiving antenna, the ability of that antenna to extract power from the incoming wave is the "effective aperture", and this depends upon the wavelength of the incoming wave. Antenna performance is more usually characterised using the antenna gain, which is the ratio of the antenna's effective aperture in the direction of the main beam to the effective aperture of an "ideal" isotropic antenna that receives signals equally well in all directions. Antennas are reciprocal devices and so their characteristics (including gain) apply equally to both transmission and reception.

These effects are collectively described by the free space path loss equation, sometimes known as the Friis transmission equation, which describes how a radio link performs in free space. The equation assumes that the antennas are optimally pointed at one another and that their polarisations match, otherwise there are further losses associated with pointing error and polarisation mismatch. The original paper (Friis, 1946) presents the equation in terms of effective aperture, and in linear units. The more commonly used version quoted here is expressed in terms of antenna gain and uses decibel units.

Equation 1, adapted from Griffiths (1987, p. 12), is the free space path loss equation in decibel units:

$$P_{rx} = P_{tx} + G_{tx} + G_{rx} - 20\log_{10}\left(\frac{4\pi d}{\lambda}\right) \qquad (1)$$

- P_{rx} is power at the receiver, in dBW (dB relative to 1 watt)
- P_{tx} is power transmitted by the transmitter, in dBW
- G_{tx} is the gain of the transmitting antenna, in dBi (dB relative to the performance of an isotropic antenna)
- G_{rx} is the gain of the receiving antenna, in dBi
- d is the distance between the transmitting and receiving antennas in metres
- λ is the wavelength of the transmission.

The last term of Equation 1 is known as the "free space path loss" (FSPL) and combines the geometric attenuation due to distance with the apparent wavelength-related attenuation caused by the effective aperture of the antennas. Consequently, the free space path loss equation gives us the rule of thumb that lower frequencies (= longer wavelengths) appear to propagate further than higher frequencies.. FSPL over 2500 m ranges from 70 dB at 30 MHz to 99 dB at 868 MHz (Table 1), depending on frequency.

System	WiSe (Smeets)	eTracer, Cryoegg (2012), Glacsweb (2013 – present)	Glacsweb (2004 –2012)	LoRaWAN	Cryoegg (2019)
Frequency (MHz)	**30**	**150**	**433**	**868**	**169**
Distance (m)					
100	42.0	56.0	65.2	71.2	57.0
500	56.0	70.0	79.2	85.2	71.0
1000	62.0	76.0	85.2	91.2	77.0
1500	65.5	79.5	88.7	94.7	80.5
2000	68.0	82.0	91.2	97.2	83.0
2500	70.0	83.9	93.1	99.2	85.0

Table 1: Values of free space path loss in dB for several frequencies used by previous subglacial wireless transmission systems (Smeets and others, 2012; Bagshaw and others, 2014; Martinez and others, 2004; Hart and others, 2019), the industrial standard LoRaWAN (Low power Radio Wireless Area Network (About LoRaWAN® | LoRa Alliance®)) and the redesign of Cryoegg (see results section).

FSPL applies to all radio links regardless of the propagating medium. However, where the medium is lossy the signal is further attenuated by the interaction between the wave and the medium. Ice is one such lossy medium. Whilst simple models can predict RF attenuation in pure ice, in reality, glacier ice is heterogeneous, varying in temperature, pore water and impurity content and it contains cracks, water pockets and debris. Ultra-high frequencies (UHF, 300 MHz–3 GHz) have been effective for transmission through deep, cold and uniform ice (Lewis and others, 2015), but any presence of water in this matrix quickly reduces success due to scattering and attenuative losses. The high frequency (HF, 3-30 MHz) and very high frequency (VHF, 30-300 MHz) bands have good penetration through ice, with wavelengths longer than typical englacial water bodies encountered along the transmission path (Smeets and others, 2012).

The attenuation of electromagnetic waves in glacial ice is reported in the study of high-energy neutrinos (Barwick and others, 2005; Barrella and others, 2011). Particle physicists and radio astronomers describe attenuation using *attenuation length* (L_α) in metres as a unit rather than the *attenuation coefficient* (α) in decibels per metre. The two are related by Equation 2 (Barrella and others, 2011):

$$L_\alpha = \frac{1}{\ln\sqrt{10^{\frac{\alpha}{10}}}}. \qquad (2)$$

We can rearrange and simplify Equation 2 to allow us to convert attenuation length to attenuation coefficient in dB m^{-1} (Equation 3). Some typical values of attenuation length are shown converted to dB per kilometre in Table 2.

$$\alpha = \frac{20}{(\ln 10)L_\alpha} \qquad (3)$$

Attenuation length (L_α), metres	**Attenuation coefficient (α), dB km^{-1}**
100	86.9
200	43.4
300	29.0
400	21.7
500	17.4
600	14.5
700	12.4
800	10.9
900	9.7
1000	8.7
1500	5.8
2000	4.3
5000	1.7

Table 2: Attenuation length and corresponding attenuation coefficient from 100 to 5000 m

Attenuation lengths determined experimentally vary slightly by frequency (Barwick and others, 2005), with lower frequencies generally having longer attenuation lengths (and hence lower attenuation coefficients). Mitigating against both free-space and ice-related losses therefore points towards the use of lower frequencies for radio links within ice. However, low frequencies imply long wavelengths, which in turn requires physically large antennas, as an efficient antenna needs to be at least ¼ of a wavelength long. The WiSe system at 30 MHz has a wavelength of 10 metres and used half-wavelength dipole receiving antennas which were five metres long (Smeets and others, 2012). Large antennas become impractical to work with in the field, and we had the additional challenge of needing to fit our transmitting antenna into the 120 mm diameter Cryoegg enclosure. Our previous work used 151 MHz (wavelength 2 m), which had given satisfactory performance and allowed the receiving antenna to be easily carried in the field. The very small size of the Cryoegg enclosure meant that there was limited value in going to higher frequencies as the benefits of having a better-matched transmitting antenna were far outweighed by the additional free-space and ice-related losses. We therefore looked for a system that could operate in the VHF band (30-300 MHz).

For frequencies in the VHF range (30-300 MHz) the attenuation lengths reported (Barwick and others, 2005; Barrella and others, 2011) range from 200 m to 3000 m. We take the worst-case figure of 200 m (43.4 dB km^{-1}) as our design criterion for working in warm, wet ice and 400 m (21.7dB km^{-1}) as a conservative estimate for cold, dry ice (Table 2).

METHODS

Choice of transmission scheme

The term "transmission scheme" encompasses all the technical aspects of the radio link – the modulation, error corrective coding, packetisation, and higher-level protocols. We required a commercially available system designed for long battery life and for sending small amounts of data over long distances, often sold as "internet of things" (IoT) systems. In particular, a number of low power wide area network (LPWAN) technologies have been developed which aim to provide long-range radio links to battery powered devices. The system we selected is Wireless M-Bus mode N1 (European Committee for Standardisation, 2013), which is intended for use in utility metering. It is designed to offer very long battery life and sends data at 2.4 kbit s^{-1}. It incorporates error corrective coding, which ensures that data received over the link does not contain errors introduced in transit, and has optional cryptographic protection for security.

The appeal of this standard is that it operates in the 169 MHz frequency band, a relatively low frequency compared with most of the other systems on the market. In Europe this 169 MHz frequency band has been opened up for general license-free use (CEPT ECC Recommendation 70-03). Wireless M-Bus is an open standard and a number of manufacturers provide implementations of it. This gives confidence that the technology will remain available, whereas with a proprietary system carries a risk of the product being discontinued.

The Radiocrafts RC1701HP-MBUS4 modem used is readily available (Digi-Key part number 1783-1048-1-ND) and offers 0.5 W (27 dBm) power output on the 169 MHz band. One module is fitted to the custom printed circuit board inside Cryoegg, configured as a transmitter. For the receiver, we use Radiocrafts RC1701HP-MBUS4 demo kit (Digi-Key part number 1783-1004-ND) with one board configured as a receiver. This board can be connected to a PC via USB and will output the decoded data received over the radio link. A Python script running on the PC applies a timestamp to the received packet data and records it in a log file. This approach avoids the need to have a source of accurate time on board Cryoegg.

Antenna selection

The transmitting antenna inside Cryoegg is constrained by the physical size of the spherical case. We sought a small antenna that had previously been proven to work on the 169 MHz band. We selected the HA.10 from Taoglas, which consists of a pair of air-cored helical elements and a matching network. To minimise use of conductive materials around the antenna, the upper hemisphere is devoted to the antenna and the remaining electronics fit into the lower hemisphere (Figure 1a). The antenna is matched to the modem module using a pair of small inductors.

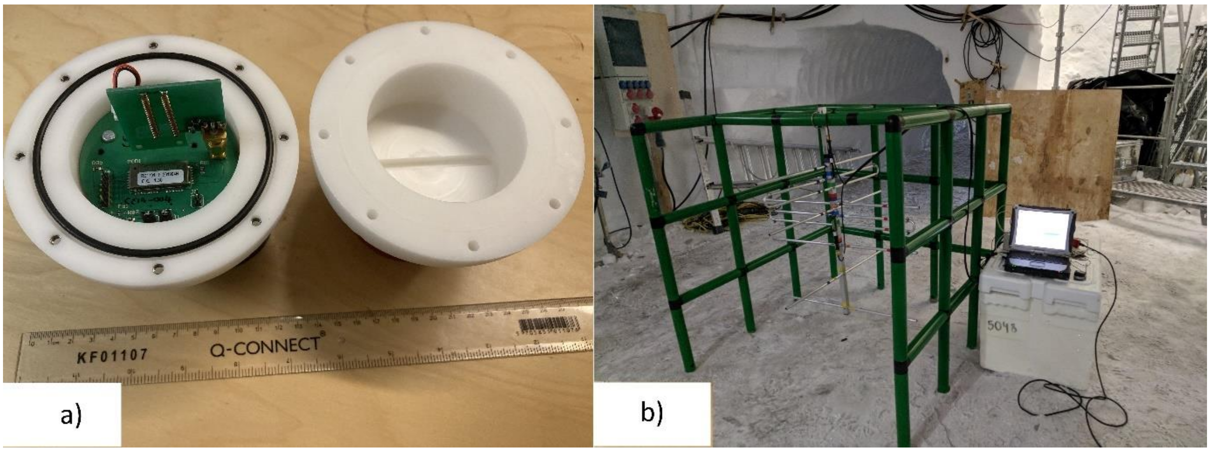

Figure 1 – a) Cryoegg with upper casework removed b) receiving antenna mounted on plastic frame

The receiving antenna on the surface provides additional gain to the system to help overcome the attenuation through the ice, and to compensate for the small size of the transmitting antenna – an ideal antenna would be 450 mm long and Cryoegg's diameter is only 120 mm. We elected to use a pair of crossed Yagi-Uda antennas (Innovantennas), which provide a gain of around 8 dB individually. They are combined through a 90° hybrid combiner (Mini-Circuits part number ZMSCQ-2-180BR+) which makes them behave as a single circularly polarised antenna, but at the expense of 3dB loss in the combiner. By transmitting with linear polarisation and receiving with circular polarisation, we make the radio link performance relatively independent of Cryoegg's orientation. This technique was also used by the WiSe project team (Smeets and others, 2012).

The receiving antenna is about one metre long. In order to minimise disturbance to the antenna pattern caused by metal parts close to the antenna elements, we used a modular plastic frame (Quadro, Hamburg) to support the antenna, as shown in Figure 1b.

The radiation pattern of Cryoegg was assessed in a screened RF test chamber (at the Wolfson Centre for Magnetics in Cardiff) lined with absorbent ferrite material to prevent multipath. A log-periodic antenna was used to receive the signal and the signal level was observed using a spectrum analyser in peak hold mode.

Link budget

A link budget is used to evaluate whether an attenuation-limited radio link will work in practice. Starting with the power output of the transmitter, gains and losses in the system are totalled up and compared to the sensitivity of the receiver. If the received power level is greater than the sensitivity, the system will work. To allow some margin for unexpected attenuation, we aim for a received power level several dB higher than the sensitivity. Link budgets are traditionally calculated in decibel units as this allows the gains and losses to be added and subtracted (rather than multiplied and divided). Hence we use decibel units of power, such as dBW: decibels relative to one watt, (0 dBW = 1W) or dBm: decibels relative to one milliwatt (0 dBm = 1mW = -30 dBW, and +30 dBm = 1 W = 0 dBW).

The link budget calculation (Table 3) assumes a 2000 m borehole through cold ice, with the attenuation coefficient estimated at 21 dB km^{-1}. The performance of the transmit antenna was relatively poor, and so we estimated its gain at -15 dBi (dB relative to an isotropic antenna) based on data from the manufacturer. For the 2000 m example shown here, the received signal margin is 10.5 dB.

			Link budget contribution	Units
Transmitter power	0.5	W	27.0	dBm
Coupling loss			-0.5	dB
Transmit antenna gain			-15.0	dBi
Distance to receiver	2	km		
Frequency	169	MHz		
FSPL			-83.0	dB
Attenuation coefficient for cold ice	21	dB/km		
Ice related loss			-42.0	dB
Crosspolarisation loss			-3.0	dB
Receive antenna gain			8.0	dBi
Total power at receiver			**-108.5**	**dBm**
Receiver sensitivity	-119	dBm		
Margin			10.5	dB

Table 3: Link budget calculation for Cryoegg in 2000 m borehole in cold ice (gains are positive values, losses are negative).

Sensors

The Keller PA-20D pressure sensor, with 250 bar maximum, has a vacuum-sealed membrane and communicates with the microcontroller via the widely-used digital I^2C interface (Inter-Integrated Circuit; (UM10204 I2C-bus specification and user manual, 2014)). It provides internal temperature compensation, and supplies a temperature reading alongside the pressure reading, although the manufacturer does not guarantee its performance at temperatures below 0 °C. Hence we provided our own independent temperature sensor, details of which are below. The sensor provides a 16-bit pressure reading to the microcontroller but uses only half the available range (the rest being used to allow it to report pressures slightly beyond the calibrated range). This means that the smallest pressure step reportable is 7.6 millibars. The nominal total error band is 1% of full scale, i.e. 2.5 bar, but in practice we found we could reliably record changes in water pressure down to 0.1 bar (1m hydrostatic pressure) during field experiments.

The temperature and EC sensors are adapted from earlier designs (Bagshaw and others, 2012, 2014). The EC sensor consists of a square wave oscillator which supplies a 500 kHz waveform to a potential divider consisting of a precision resistor and a pair of sense electrodes. The sense electrodes are a pair of M3 stainless steel hex-headed bolts that protrude through the case. The AC waveform from the midpoint of the potential divider passes through a precision rectifier and RC filter to produce a DC voltage that varies inversely with EC between the sense electrodes. This is sampled by the microcontroller’s analogue-to-digital converter (ADC) and the resulting digital value is reported over the radio link. The temperature sensor is a Pt1000 platinum resistance device, used in a full-bridge configuration with three fixed resistors. It is driven by a current source and measured using an instrumentation amplifier, with the output fed to the microcontroller’s ADC. Cryoegg reports the digital value from the ADC over the radio link, allowing calibration to be carried out externally. The Pt1000 resistor is mounted to the back of one of the EC sense electrodes with a thermal pad, ensuring that has thermal but not electrical contact.

Microcontroller selection

To maximise battery life, system power consumption should be as low as possible between measurements. Cryoegg therefore has a "sleep" mode where all systems were powered down apart from a system timer that wakes the main processor back up in time for the next measurement. The STM32L433RCT6P microcontroller (STMicroelectronics) has a built-in timer (known as the Real Time Clock module, RTC) which uses an external quartz crystal oscillator to provide reliable timekeeping at very low power. The RTC draws around 500 nA at 3.3 V with the rest of the microcontroller shut down. The microcontroller has a 32-bit ARM Cortex M4 processor that can be clocked at up to 80 MHz, 256 kB of flash memory and 64 kB of RAM. It has a wide range of internal peripherals, of which we use the ADC for the temperature and EC sensors; I^2C interface for the pressure sensor; and Universal Asynchronous Receiver/Transmitter (UART) for communicating with the radio module. The microcontroller also controls several power switches that enable and disable power to other parts of the circuit.

Power supply design and power consumption

The radio modem module has relatively high power consumption during transmit – requiring 500 mA at 3.3 V for less than 500 ms during each transmission, which puts a lot of demand on the battery and power supply to be able to supply this peak current. A lithium-polymer rechargeable pouch cell can supply sufficient peak current and be recharged between tests. The battery selected has a 3.7 V nominal voltage and a capacity of 400 mAh.

Power from the battery is supplied unregulated to the microcontroller, and (via a MOSFET switch) to the radio module. Using the unregulated supply means that no power is wasted by a regulator in standby mode. However, we found that a regulated supply was necessary for the sensors, since variations in battery voltage could affect their performance. A regulator IC with an enable input (ON Semiconductor NCP115ASN330T2G) supplies 3.3 V to the sensors when enabled, and also provides the ADC reference voltage to the microcontroller.

To estimate the battery life, we measured the power consumption of Cryoegg during transmission and during sleep mode in the lab, using a logging multimeter (Mooshim Engineering Mooshimeter) that could measure voltage and current from the battery simultaneously. The measure-and-transmit cycle takes 3.2 seconds and consumes 0.5 J. The sleep mode current consumption proved to be too low for the meter to measure (the lowest current it can record is 5 µA). We therefore assume that the sleep mode current consumption is that of the microcontroller only (since everything else is disabled) and take the value quoted in the microcontroller datasheet of 500 nA.

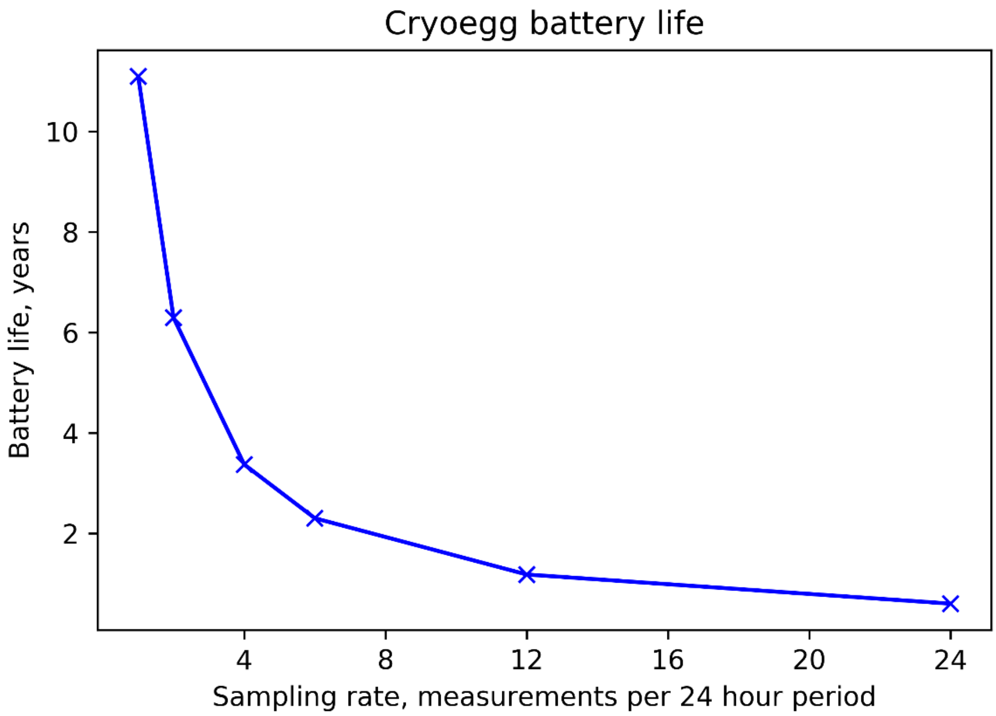

Figure 2 - Cryoegg battery life with varying sampling rate

Figure 2 shows the results of the battery life calculations. The projected battery life is over 6 years at two measurements per day. Even allowing for some self-discharge in the battery, this gives scope to increase the measurement frequency. A measurement every 2 hours (i.e. 12 times per day) gives a battery life of just over a year. Table S1 in the Supplementary Information shows an example battery life calculation in more detail.

Mechanical design

We aimed to provide a simple and robust mechanical design that was straightforward to assemble for testing. The spherical casework is machined in two halves from acetal copolymer, a hard engineering plastic. The internal void is cylindrical, as shown in Figure 1a. The lower hemisphere has a flat side through which the sensors are mounted. The sensor PCB sits directly onto the bottom of the internal void and is secured in place by two M3 threaded spacers. We used Raytech Liquid Rubber potting to enclose the sensor PCB to help prevent leaks. There are two further PCBs that mount above the sensor PCB, which interconnect using multiway connectors. The processor PCB contains the microcontroller and associated components, and also provides mechanical support for the battery. The radio PCB is uppermost and supports the radio module, antenna connector, battery connector and headers for programming and debugging. The battery, a pouch cell, is sandwiched in the gap between the radio and processor PCBs. The antenna PCB connects to the radio PCB via an SMA connector and is supported by a groove in the crown of the upper hemisphere. This design allows the upper hemisphere to be easily removed for access to the electronics, and to connect the battery before deployment. The upper and lower hemisphere seal with a rubber O-ring and are held in place by eight machine screws.

Software

The software on the Cryoegg microcontroller is written in C, using the STM32 Hardware Abstraction Libraries. The software goes through the following steps:

- Power up the sensors
- Make measurements
- Power down the sensors
- Power up the radio module
- Pack the sensor data into a data packet
- Send the data packet to the radio module to be transmitted
- Power down the radio module
- Set the sleep timer for the next measurement
- Enter deep sleep (“SHUTDOWN”) mode

On awakening from SHUTDOWN mode, the program restarts from the beginning, thus giving an endless loop. The measurements are transmitted immediately after being made, and no data is stored on Cryoegg, since we do not expect to retrieve Cryoegg after deployment. This does also mean that any data transmitted by Cryoegg that is not received on the surface is lost.

Field testing

We conducted three field tests during July and August 2019 at two sites in Greenland (EastGRIP drill site and Sermeq Kujalleq/Store Glacier) and one in Switzerland (Rhône Glacier).

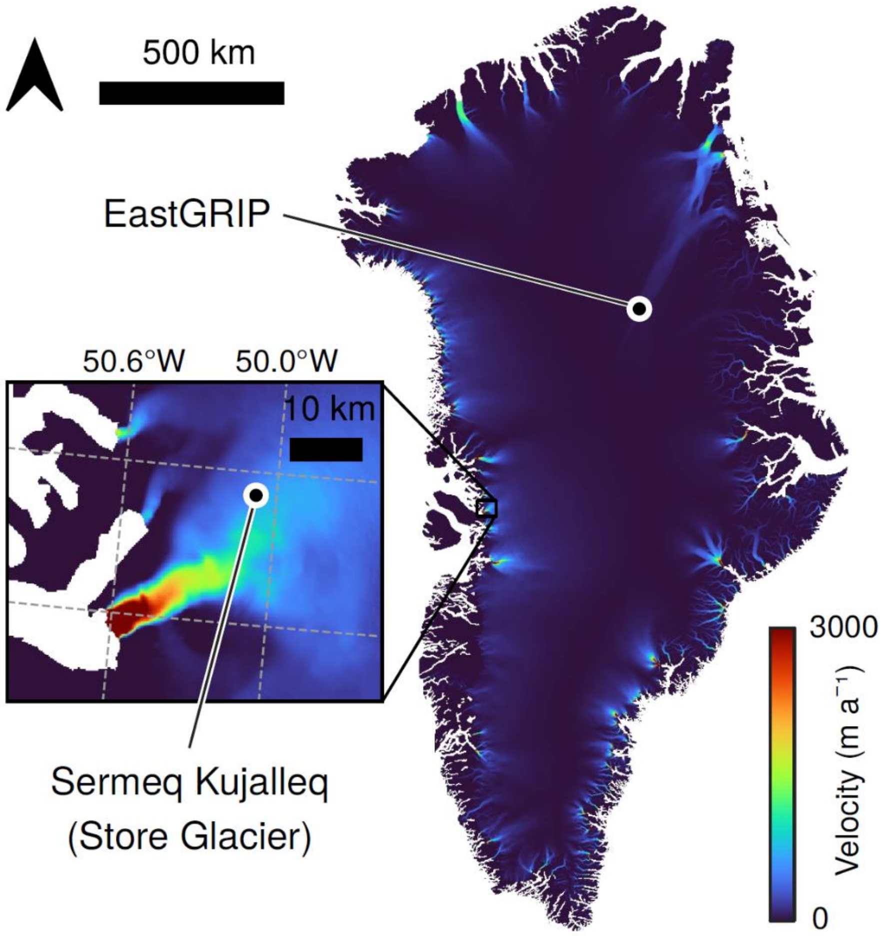

Figure 3 - Velocity map of Greenland ice sheet flow, showing locations of EastGRIP and Sermeq Kujalleq test sites in fast flowing ice. Data from MEaSUREs dataset of annual Greenland velocity for 2018 (Joughin and others, 2010; Joughin, 2017).

East Greenland Ice Core Project site (EastGRIP)

EastGRIP is located at N75° 38.05' W036° 00.22' on the North East Greenland Ice Stream (NEGIS), the largest ice stream in Greenland, which drains 340,000 km^2 of the ice sheet and extends for over 1000 km inland (Figure 3). Approximately 150 km from the onset, it reaches speeds of 65 m a^{-1} (Joughin and others, 2010; Karlsson and Dahl-Jensen, 2015). The NEGIS is the location of the East Greenland Ice core Project (EastGRIP), a unique project drilling an ice core into 2.5 km of fast flowing ice to investigate ice stream beds (www.eastgrip.org). In summer 2019, the core had been drilled to 2 km depth, leaving behind a 2 km borehole filled almost completely with drill fluid. The purpose of our field trial at this site was to obtain a range test for the radio link and a pressure test for the mechanical design. Cryoegg was deployed in a mesh bag and attached to the main winch (see Figure 4). The receiving antenna was set up in the drill trench, close to the winch (see Fig. 1b). Cryoegg was lowered and raised into the borehole several times and the received signal strength (RSSI) and live data stream monitored at the surface, adjacent to the top of the borehole.

Figure 4 – Cryoegg ready for deployment on the EastGRIP ice core winch.

RESPONDER site at Sermeq Kujalleq

We tested Cryoegg at an inland site (N70° 33.889' W50° 04.558') at Sermeq Kujalleq (Store Glacier), the third fastest outlet glacier in West Greenland (Figure 3). It has a catchment of 35,000 km^2 that includes supraglacial lakes that periodically drain via cracks and moulins, several on an annual basis (Chudley and others, 2019). The glacier experiences changes in ice flow associated with sudden injections of meltwater to the pressurised drainage system (Doyle and others, 2018), but the link between surface lake drainage and the subglacial hydrology is poorly defined, primarily because instrumenting a draining lake with cabled sensors is near-impossible. There is extensive supporting data available on the subglacial bed structure, lake drainage frequency and ice strain rates (Hofstede and others, 2018; Young and others, 2018; Chudley and others, 2019). Sermeq Kujalleq is the site of the RESPONDER project, offering access to the glacier bed through hot water drilling. The glacier is approximately 1 km thick at this site (Morlighem and others, 2017), and bed access holes were hot water drilled in July 2019.

A surface propagation test assessed the range of data transmission through air by monitoring the RSSI and live data stream as the receiving antenna was deployed at a fixed site and Cryoegg hand-carried over a distance of 1.6 km. A hand-held GPS receiver was used to record the position of Cryoegg as it was carried, and the fixed position of the Cryoegg receiver.

Rhône Glacier site

Figure 5 – topographic map of Switzerland showing location of the Rhône Glacier

The Rhône Glacier is located at N46°34.32′ E8°22.58′ in the Swiss Alps and is one of the most studied glaciers, with records of front position dating back to the 17^{th} Century (Church and others, 2019). The 16 km^2 glacier is at the pressure melting point throughout and there is an active subglacial drainage network. The glacier is the focus of an intensive subglacial monitoring project, with artificial moulins drilled via hot water in 2018. The moulins remained active in August 2019, when we deployed Cryoegg on the end of a rope tether.

Salt dilution gauging (Moore, 2005) was used to estimate moulin discharge. A known quantity of tracer, sodium chloride (NaCl, “table salt”) was added to the supraglacial stream approximately 25 m upstream of the moulin. The discharge can then be calculated from EC readings and the concentration of NaCl added. EC was measured in the supraglacial stream by a Keller DCX-22-CTD 15 m upstream of the moulin and also recorded and transmitted once per second by a Cryoegg lowered into water at the bottom of the moulin.

RESULTS

Laboratory RF tests

RF power meter assessments confirmed that the transmitter put out the full +27 dBm (0.5 W) during each transmission.

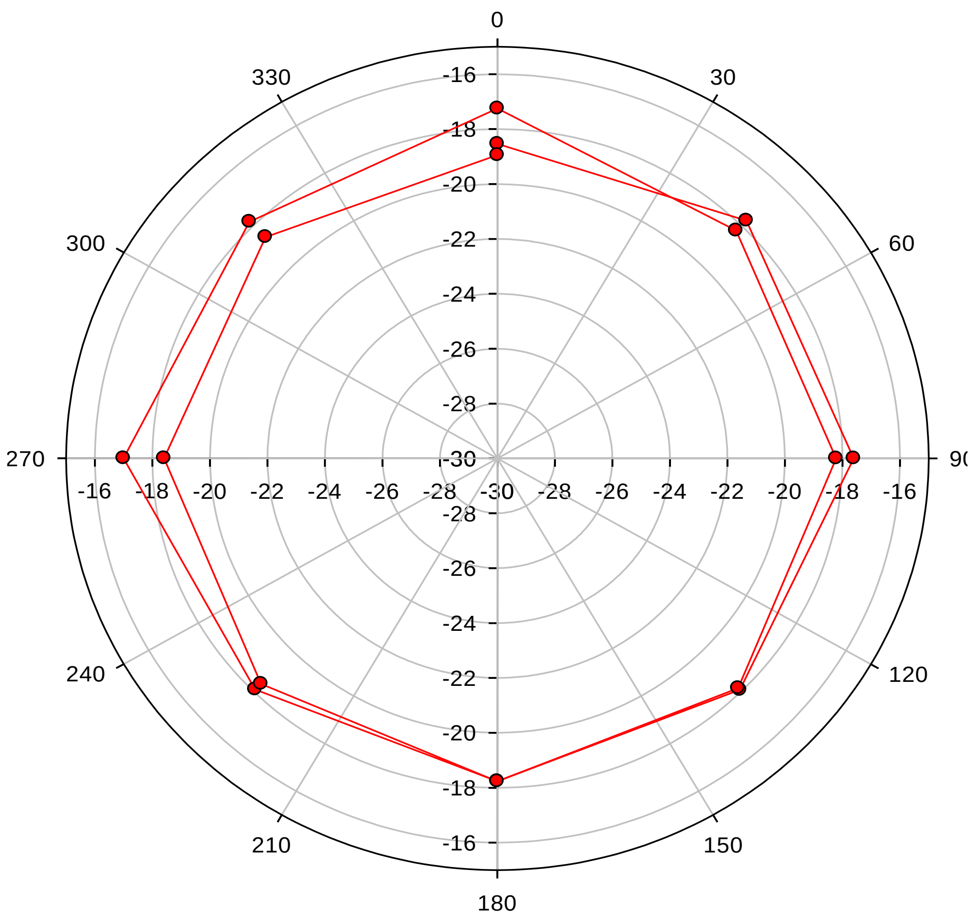

Figure 6 – Horizontal radiation pattern of Cryoegg measured in the RF test chamber

The horizontal radiation pattern was measured at eight points around the circumference and is shown in Figure 6. For this measurement the receiving antenna (a log-periodic) was vertically polarised (a brief check showed that this gave a larger signal than when horizontally polarised) and Cryoegg was orientated with its case split line horizontal. Two complete revolutions were measured to check consistency, and it is clear that the pattern is largely omnidirectional, varying by < 2 dB.

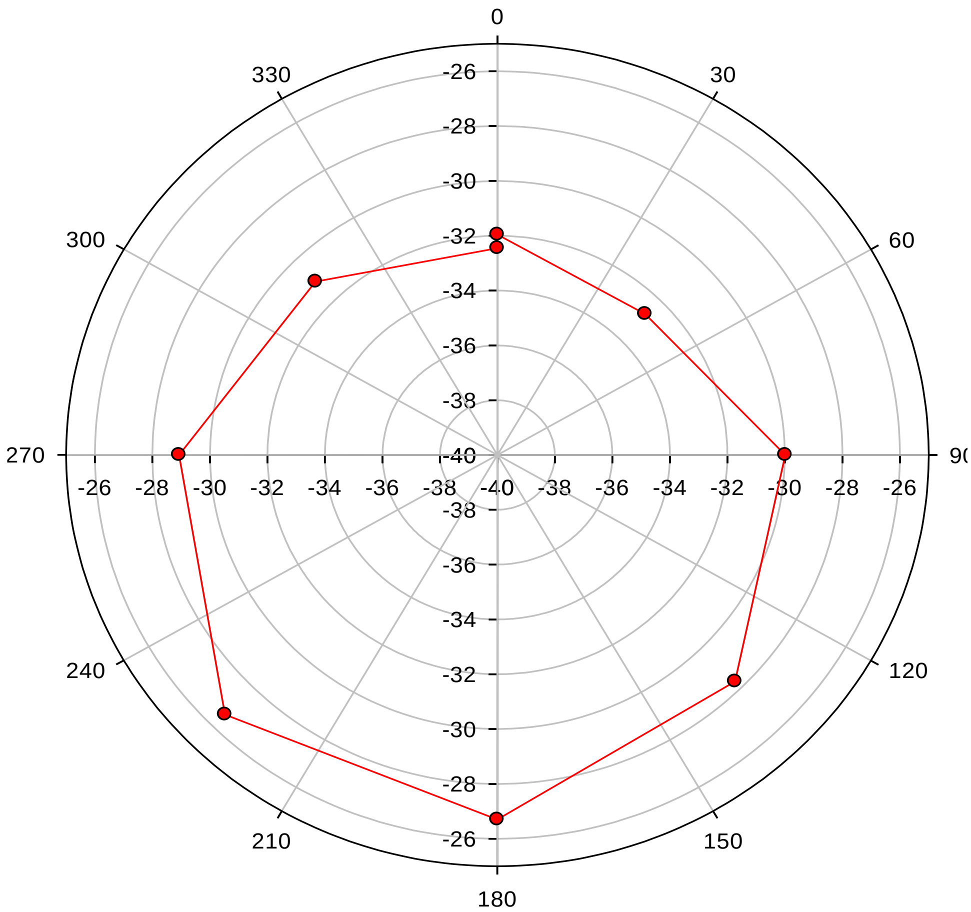

Figure 7 – Vertical radiation pattern of Cryoegg measured in the RF test chamber

To simulate the RF performance in the borehole, we re-oriented Cryoegg to have the same orientation as it would have in the borehole, with the split line vertical and normal to the receiving antenna boresight – i.e. with the crown of the upper half pointing towards the receiving antenna, and the sensor ports pointing away. The receiving antenna was vertically polarised. The results in Figure 7 show that the signal level is significantly lower (10-12 dB) than in the horizontal plane, and that the pattern is not omnidirectional; there is a 6 dB variation as the unit is rotated.

Surface propagation at Sermeq Kujalleq

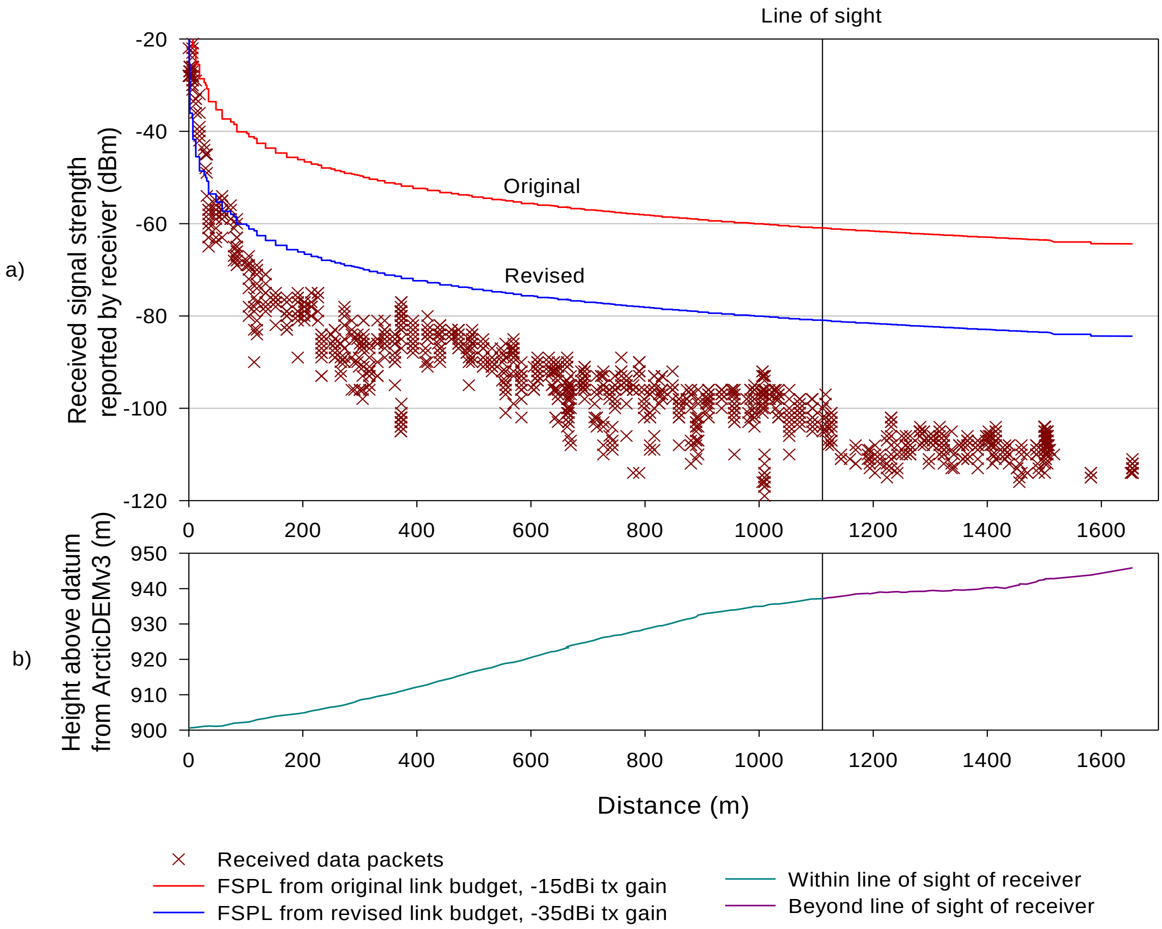

Figure 8 – a) RSSI recorded by receiver during surface range test at Sermeq Kujalleq and expected received signal strength based on original and revised link budget models (explained in text). b) shows the ground elevation along the route taken. The black vertical line in both plots shows the point where the transmitter went beyond the line of sight to the receiver due to the glacier surface topography.

Figure 8a shows recorded signal strength for successfully received data packets against range from the receiver. The terrain profile in Figure 8b was produced from ArcticDEM v3 (Porter and others, 2018) 2 m mosaic values extracted to match the GPS positions recorded in the field. A line of sight binary was calculated using the QGIS visibility analysis plugin with the receiver height set at 1.5 m and the transmitter height at 1 m. Given that propagation was mostly in air, and ground reflection on glaciers is negligible, we expect the signal strength to drop off according to the free space path loss equation.

Deployment at Sermeq Kujalleq

Cryoegg was lowered into a hot water drilled borehole and a moulin. One deployment attempt was made in the hot water drilled borehole, but the borehole proved too narrow for Cryoegg to pass through. One data point was obtained with Cryoegg in the borehole about 400 m below the surface, but it was impossible to proceed further because of borehole refreezing. Moulin deployment was attempted in a very large moulin (measured at 4.3 m^3s^{-1} discharge at the time of deployment) adjacent to the drill site. Cryoegg was caught in a series of plunge pools and eventually the force of the water caused it to break free from its tether and it was rapidly swept away out of range. We only obtained a few data points before losing the signal.

Downhole propagation at EastGRIP

At EastGRIP, the borehole is filled with ESTISOL 240 drill fluid rather than water (Sheldon and others, 2014). Previous tests at the site (Bagshaw and others, 2018) demonstrated that the fluid had minimal impact on signal propagation. Figure 9 shows the RSSI plotted against depth. Depth is linearly interpolated between depth-measured winch halt points (shown as vertical gridlines on Figure 9), which is a fair assumption because the winch motor speed was constant between these halts. The firmware was configured to produce a burst of 16 packets, one per second, and then wait for 60 seconds before the next burst. This accounts for the clustered data points on Figure 9, as all the successfully received packets are plotted.

If the transmitted power output from the Cryoegg antenna was constant, and the antenna radiated equally in all directions, and there is no multipath, the plot should be monotonic, with the signal strength always decreasing with depth. However, we can see considerable variations and even retrograde paths, for example between 400 and 500 m; 700-850 m; 1000-1100 m. There are also large variations (>10 dB) in signal level at 300, 400 and 500 m, coinciding with the point where the winch was halted.

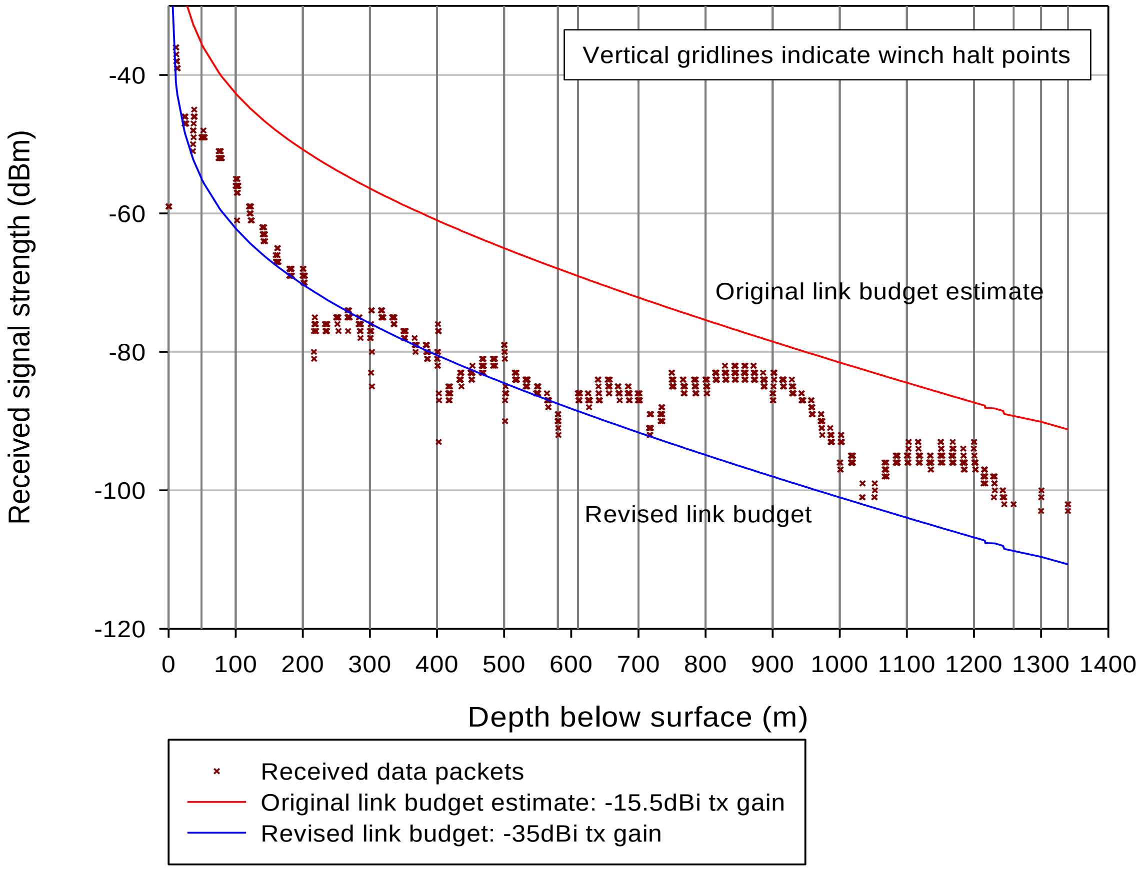

Figure 9 – Received signal strength of successfully-received data packets during a test in the EastGRIP borehole, together with estimated signal strengths produced by link budget calculations.

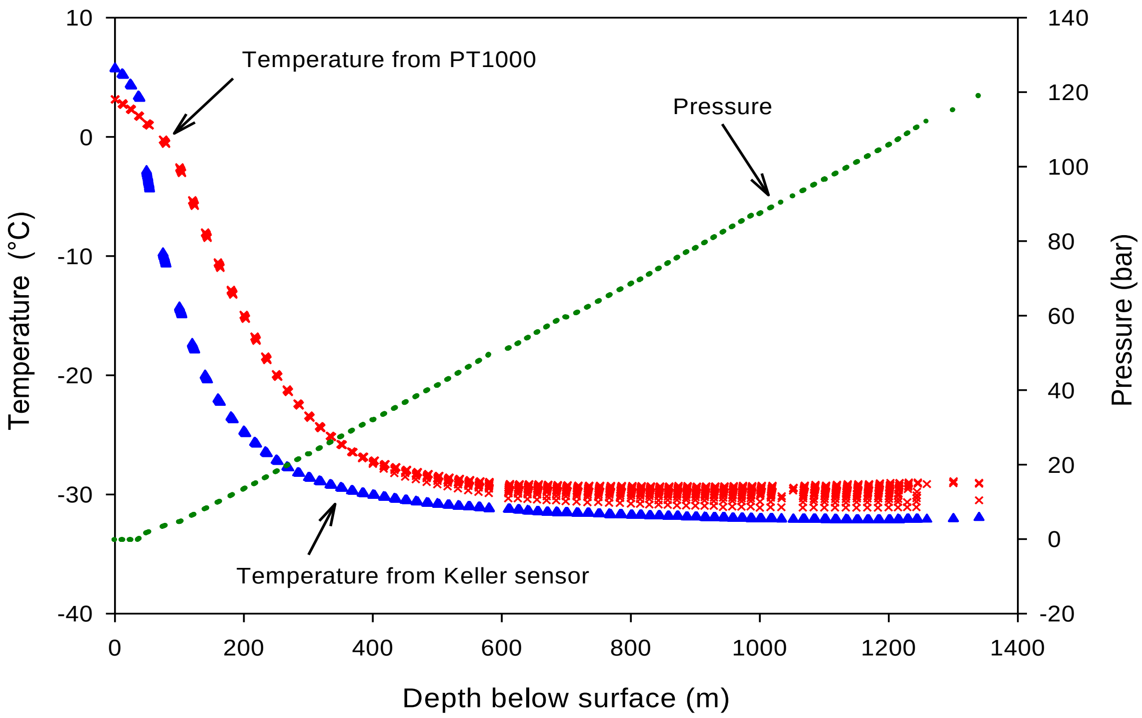

Figure 10 – Data received from Cryoegg sensors during the same test in the EastGRIP borehole as Figure 9.

Data from the sensors is shown in Figure 10. The hydrostatic pressure increased with depth – the small offset is because the drill fluid is around 50 m below the surface level. Data was obtained down to 1340 m, although significant packet loss occurred beyond 1250 m. The two temperature plots represent data from the two different temperature sensors. The Pt1000 sensor is inside the case, hence it records a higher temperature for a given depth. The conversion equation from the reported value (which is in arbitrary units) to temperature is based on theory and has not been confirmed by calibration. The Keller pressure sensor contains its own temperature sensor, which it uses internally to compensate the pressure readings against variations in temperature. The high degree of clustering of the points suggests that the Keller sensor contains some internal averaging, although this may be caused by the significant mass of the sensor body itself. It is worth noting that Cryoegg was warm before entering the borehole, so the majority of the temperature data recorded here is simply the instrument cooling down to the ambient englacial temperature.

Moulin drainage at Rhône Glacier

Cryoegg was not able to reach the bed of the Rhône Glacier, 200m below the surface, but instead appeared to be in a deep plunge pool 150m below the surface. Pressure readings received from Cryoegg in real time confirmed that the egg was in up to 25m deep water. Figure 11 shows the pressure recorded whilst Cryoegg was in the plunge pool, and the corresponding received signal strength. There was a sharp rise in pressure as Cryoegg was lowered into the water at 13:12:00 UTC and then a gradual decline over the next 40 minutes. The gap in the data centred on 13:55 was an interruption in the data logging. After the logging resumed, the water pressure had fallen to atmospheric pressure. The reduction in water pressure coincided with a 10dB increase in received signal strength over the same period.

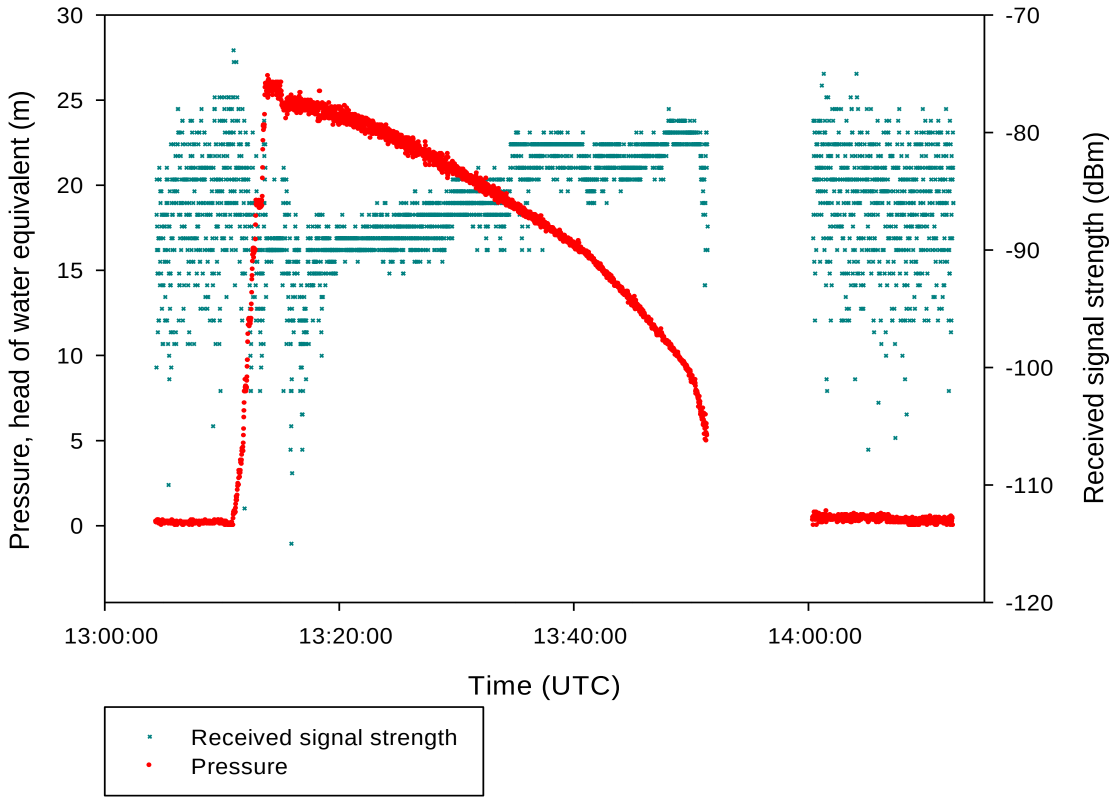

Figure 11 – Pressure and received signal strength from Cryoegg when tested in a moulin on Rhône Glacier, 15th August 2019

Salt discharge gauging at Rhône Glacier

Figure 12 shows an example of EC changes as a salt wave passes the Cryoegg, transmitted in real time from the moulin plunge pool at 150 m below the ice surface.

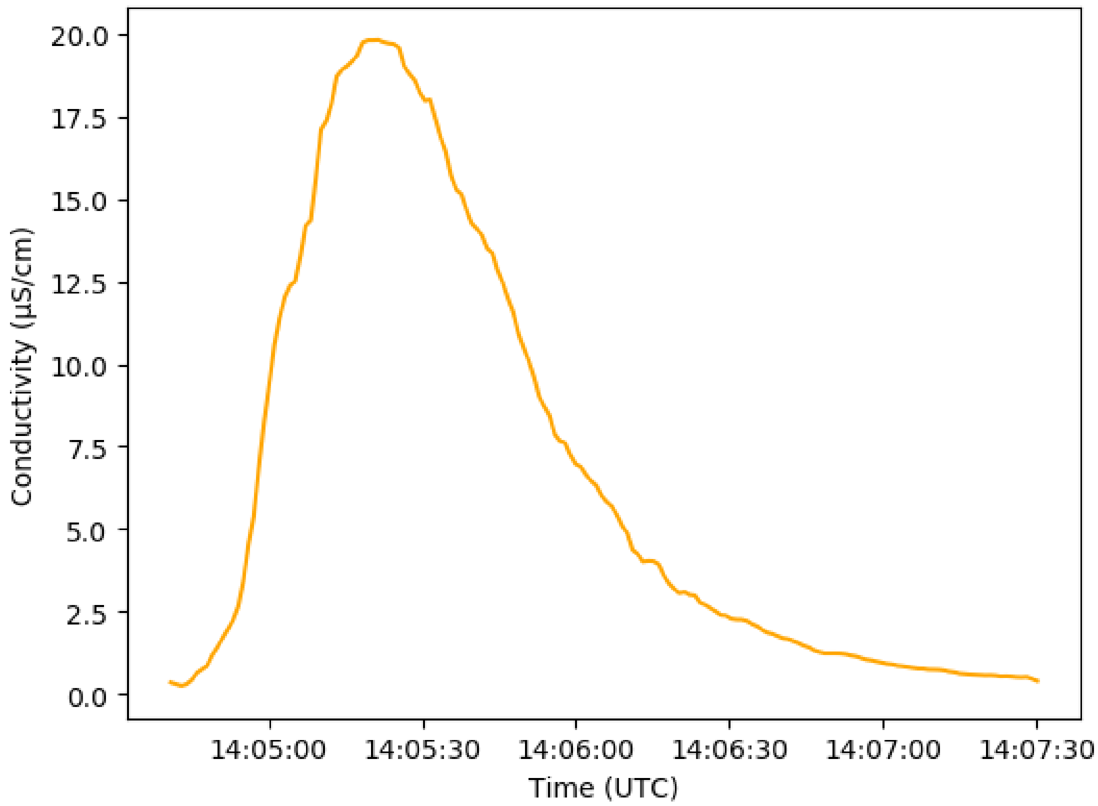

Figure 12 – reported EC from Cryoegg from within a moulin on Rhône Glacier during a salt slug injection test, 15th August 2019.

Simultaneously, the Keller DCX-22-CTD in the supraglacial streams that fed into this same moulin measured the injection of the 100 g l^{-1} NaCl salt solution 10 m upstream from the logger. Figure 13 shows the results from the Keller logger in the stream alongside the results from Cryoegg in the moulin.

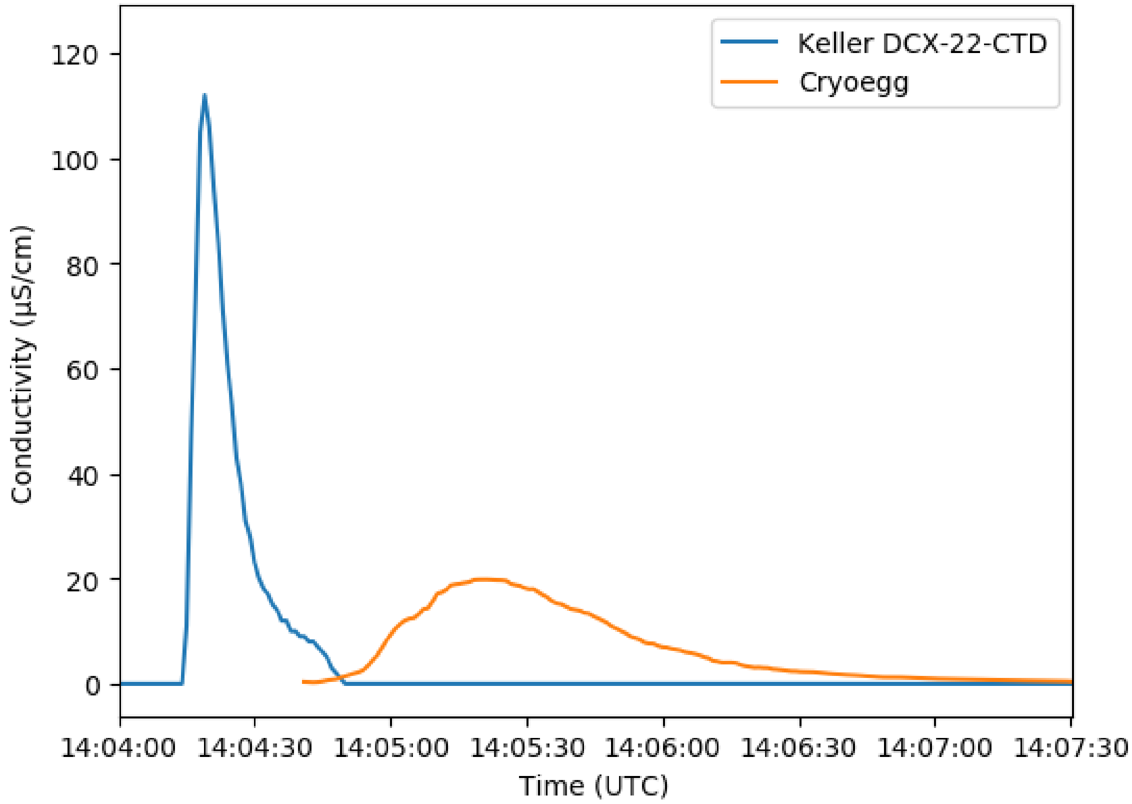

Figure 13 – comparison of salt wave passing Keller logger in the supraglacial stream with Cryoegg within the moulin. 15th August 2019.

The discharge of the supraglacial stream was calculated by the salt dilution as 104 litres s^{-1} (Moore, 2005), and the discharge within the moulin was slightly higher at 113 litres s^{-1}. The time between the two peaks was 60 seconds. The velocity of the water between the two instruments was 2.75 m s^{-1} based on the transit time and the distance between them (15 m in the stream + 150 m down the moulin = 165 m).

DISCUSSION

Radioglaciological implications

The surface range test at Sermeq Kujalleq (Figure 8) indicates that the radiated RF power output of Cryoegg is less than we intended. The upper curve ("Original") indicates the expected performance for propagation in air if link budget (Table 3) assumptions were correct. In practice the performance is at least 20 dB lower than the original link budget and deteriorates with distance. There are several factors at play here. The main issue appears to be the performance of the transmitting antenna, which is unsurprising since it is electrically very small. We verified experimentally (see "Laboratory RF tests", above) that the radio module outputs the full +27 dBm, so the lack of output suggests that the antenna is poorly matched to the 50-ohm feed from the radio module, causing power to be wasted. We also verified that the radiation pattern from the antenna is not uniform (Figure 7), which accounts for some of the variations in signal level. Some of the variations in signal level are also terrain-related: it was not practicable to move in a straight line away from the receiving antenna because of crevasses and meltwater streams, so there will be some variation introduced from the radiation pattern of the receiving antenna. Whilst the early part of the test consisted of a gradual ascent up the slope of the glacier, there were numerous ridges and valleys in the surface which had to be climbed over, and these would have resulted in the signal being attenuated by the ice surface. The later part of the test was beyond the line of sight to the receiver (as shown by the elevation profile in Figure 8b), which accounts for the step reduction in signal level beyond 1100 m.

We considered the performance in the EastGRIP borehole to be acceptable for a first attempt. We propose a number of candidate explanations as to why no data was received beyond 1340 m depth:

- Mechanical failure: we know that drill fluid entered the Cryoegg housing during the tests because residues were found inside the housing afterwards. The pressure from the drill fluid is likely to have affected the internal electronics. Of particular concern are the battery (which being a soft "pouch cell" type has no protection from pressure) and connectors, which may be forced apart by non-conductive fluid under high pressure, breaking the circuit.
- Electrical noise at the receiver prevented weak signals being received
- Antenna performance: the antennas (transmitting and receiving) provided insufficient gain
- Ice properties: the attenuation of the ice might be greater than previously thought

The receiver gives an indication of received signal strength (RSSI, dBm) for each packet that is successfully received. The receiver data sheet (RC1701xx-MBUS Datasheet, 2018) indicates that the sensitivity (the minimum decodable signal strength) is -119 dBm (1.25 fW), and in other range tests (the surface range test in Figure 8) we succeeded in decoding signals down to this level. However, the RSSI data for the EastGRIP borehole (Figure 9) show that the weakest signals received were only at -103 dBm, 16 dB above the minimum receivable level. Whilst we might have expected a small performance reduction because the site at EastGRIP has electrically noisy machinery, this would not usually account for 16 dB of lost performance. This therefore points more towards a mechanical problem being the primary cause of failure rather than an RF issue, especially given the presence of drill fluid inside the Cryoegg housing at the end of the tests.

The output of the original link budget model (Table 3) for the propagation at EastGRIP is shown in Figure 9. This model includes both free-space loss and 21 dB km^{-1} of ice-related loss. It is clear from both the Sermeq Kujalleq range test (Figure 8) and from the EastGRIP test (Figure 9) that the radiated output from Cryoegg was at least 20 dB lower than was allowed for in the original link budget. Replotting the link budget using the same value (21 dB km^{-1}) for the ice attenuation coefficient but adjusting the transmit power down by 20dB produced the "revised link budget" curve plotted on

Figure 8 and Figure 9. This fits closely to the data up to around 600 m, where ice-related attenuation is still a relatively small factor, suggesting that the transmit power estimate is broadly correct. Beyond 600 m the revised link budget becomes a conservative estimate for the performance in deep ice. It is highly likely that the attenuation coefficient is not constant throughout the borehole, but for our purposes we require a realistic but conservative estimate for the ice attenuation in order to be sure of the link performance in future iterations of the Cryoegg design. The first 90 m of the borehole is surrounded by firn (Vallelonga and others, 2014, (Fig. 9)), whereas the lower section is in glacier ice, and the changes of material properties both from firn to ice and within the ice itself will cause some variation in attenuation coefficient (Bagshaw and others 2018). These variations notwithstanding, this data confirms that 21 dB km^{-1} (see section "Choice of frequency / radio propagation in ice" above) was a safe choice for the ice attenuation coefficient in our link budget.

The large (>10 dB) variation in signal strength observed at several winch halt points is most likely caused by Cryoegg rotating on the vertical axis as the wire rope twists. The deceleration of the winch will result in some of the momentum of Cryoegg and the cable being converted into torsional forces on the winch cable, with Cryoegg twisting back and forth on the end of the cable. This then indicates that the antenna radiation pattern is not as uniform as we had hoped and is perhaps also being adversely influenced by the presence of the metal winch cable. The non-uniformity of the radiation pattern is confirmed by our laboratory tests (Figure 7).

The signal strength plot (Figure 9) appears to show a number of nulls – locations where the signal strength drops significantly – notably at around 600 m and 1040 m. Nulls are often produced by multipath effects, where the signal reflected off a surface interferes destructively with the direct signal at the receiver (Griffiths, 1987, 102–104). However, in this case there is no obvious candidate for the reflecting surface: the geometry required to produce widely-spaced large nulls rules out horizontal reflectors like the glacier bed or internal layers. The shear margin is too far away (5 km) to produce this type of null. More data will be required to determine whether these nulls are equipment related or caused by some property of the ice stream's structure.

The performance of the radio link in the Rhône glacier moulin (Figure 11) was also satisfactory. We anticipated that the temperate ice and presence of flowing water would increase the overall attenuation. Figure 11 shows that the signal propagating through 25 m of meltwater and a further 125 m of temperate ice to the glacier surface was attenuated to -90 dBm. This compares with the EastGRIP borehole (Figure 9) where this signal strength was reached after more than 500 m. The reduction in observed moulin water pressure, indicative of 25m head of water draining out of the moulin, produced an increase in RSSI by around 10 dB. This confirms that the presence of liquid water increases the signal attenuation.

The variation in signal is much greater when Cryoegg is in the "atmospheric pressure" region of the moulin rather than when it is in >1 m of water (Figure 11). When Cryoegg is reporting pressure close to atmospheric pressure, it is being splashed by the water, or water is flowing smoothly past it. In this scenario the water flow will spin and agitate Cryoegg on the end of the rope, creating variation in signal level because of the antenna pattern. The turbulent flow of the water will also create ever-changing levels of attenuation. However, once Cryoegg is below the water surface, the viscosity of the water will reduce its spinning and agitation, and the attenuation due to the water will be constant.

Glaciohydrological implications

The water pressure recorded by Cryoegg in the moulin steadily decreased during the 40 minutes that it remained in the plunge pool (Figure 11). Eventually, the water level dropped below Cryoegg and it returned to atmospheric pressure with the characteristic fluctuations in RSSI caused by splashing water. We interpret this as dynamic drainage of the plunge pool over the afternoon, as water backed up in the drainage system forces its way to the glacier bed. Similar pressure variations have been previously observed in moulins (Iken, 1972; Röthlisberger, 1980; Holmlund and Hooke, 1983) and demonstrate that the subglacial drainage system is not in equilibrium but constantly fluctuating (Röthlisberger and Lang, 1987). The characteristic step-pool system develops if the moulin persists for more than one season (Gulley, 2009); the artificial moulin was drilled directly to the end in 2018, but by 2019 was 'kinked' and a plunge pool formed approximately 50 m above the bed.

Simultaneous salt tracing in a supraglacial stream feeding the moulin and within the moulin itself shows (Figure 13) that the moulin discharge was slightly higher than the stream discharge – unsurprising, as the stream that we measured was not the sole supply of water feeding the moulin. This experiment demonstrates Cryoegg's potential for measuring hydrological parameters in locations that are difficult to access. Previously, moulin discharge has been estimated at the surface (either by field measurements or remote sensing), which masks the effect of water being stored within the vertical column of the moulin itself (Werder and others, 2010). We show that it is possible to monitor supraglacial discharge, the height of the stored water column within the moulin, and the moulin discharge simultaneously and in real time, providing a valuable new approach for future studies of glacier hydrology.

Comparison with other wireless subglacial probes

The most successful wireless subglacial probe for deep ice has been the WiSe system (Smeets and others, 2012). This was demonstrated returning a signal through 2500 m of ice in Greenland. This system operated at 30 MHz in order to benefit from lower free-space attenuation, but at the expense of making the antennas very large. The WiSe system suffered from some skywave interference affecting signal reception, which is a particular issue at 30 MHz and below, and required use of a large (5 m long) HB9CV type antenna to mitigate against it. WiSe required a 1 W (+30 dBm) transmitter to communicate at depths of more than 2000 m, but it is not clear not how much of this power was actually radiated – the ferrite-loaded antenna used was likely to be very lossy.

Our probe and receiving antenna are both more compact than the WiSe system and we use commercially-available radio modules that adhere to an international open standard, which means that the key components are likely to be readily available well into the future.

The GlacsWeb system originally operated at 433 MHz (Martinez and others, 2004) but later (Martinez and others, 2013) used 151 MHz, giving a maximum reported range in ice of 70 m (Hart and others, 2019). Cryoegg is specifically designed for deep ice, and hence our radio performance greatly exceeds that of GlacsWeb, enabling its use in at least 1000 m of ice.

CONCLUSION AND OUTLOOK

We have undertaken a full re-design of the wireless subglacial sensor platform Cryoegg, using a new radio link technology and improved link budget design, and demonstrate that it can transmit sensor data in real time through more than 1.3 km of cold ice. Deployments in moulins in temperate ice show that Cryoegg is a valuable tool for recording englacial and subglacial hydrological properties in situ, and hence giving further insight into processes in these environments. The EC sensor, originally intended as a proxy for total dissolved solids in subglacial water, can facilitate salt dilution gauging for estimates of discharge. Real-time data transmission made for efficient fieldwork, allowing immediate confirmation of equipment operation and information about the target environment. All sensors operated well, revealing englacial conditions and demonstrating their applicability for future subglacial deployments. The sensors fitted to the existing design were chosen because of their ease of implementation and their applicability to studies of subglacial hydrology, but Cryoegg can be adapted to support other sensors.

Future developments will refine and enhance the design, particularly with respect to the antenna performance and mechanical design, so that we have a robust instrument capable of returning data for months or years through 2.5 km of ice. This would enable us to match the performance of the WiSe system (Smeets and others, 2012) but with more compact antennas, enabling the Cryoegg to 'roam' through englacial and subglacial hydrological systems to collect spatially and temporally distributed measurements, reported in real time. Cryoegg technology will also be adapted for englacial studies in irregular and refreezing hot-water-drilled boreholes, by creating a cylindrical form factor with a much smaller diameter than Cryoegg, allowing deployment in a smaller borehole.

ACKNOWLEDGEMENTS

This work was funded by UK Engineering and Physical Sciences Research Council (EPSRC) New Investigator Award EP/R03530X/1.

Thanks to all who assisted us in the field, in particular: Trevor Popp, Romain Duphil and the EastGRIP drill team; "Mickey" MacKay, Eliza Dawson and Rob Law at the RESPONDER site; Lai Bun Lok, Jonathan Hawkins, the ETH Zürich VAW Glaciology team and the Swiss Air Force at the Rhône Glacier site. Phil Anderson gave us use of the RF test chamber. We are grateful for in-kind contributions of equipment from Quadro and Radiocrafts. Particular thanks to the team at DGF Engineering for the machining of the caseworks, and to Protronix EMS Ltd for the rapid production of the electronics. Miles Gould provided assistance with the algebra for Equation 3.

EastGRIP is directed and organized by the Center of Ice and Climate at the Niels Bohr Institute. It is supported by funding agencies and institutions in Denmark (A. P. Møller Foundation, University of Copenhagen), USA (US National Science Foundation, Office of Polar Programs), Germany (Alfred Wegener Institute, Helmholtz Centre for Polar and Marine Research), Japan (National Institute of Polar Research and Arctic Challenge for Sustainability), Norway (University of Bergen and Bergen Research Foundation), Switzerland (Swiss National Science Foundation), France (French Polar Institute Paul-Emile Victor, Institute for Geosciences and Environmental research) and China (Chinese Academy of Sciences and Beijing Normal University)

Bryn Hubbard acknowledges support for hot-water borehole drilling from HEFCW through a Capital Equipment Grant awarded to Aberystwyth University, and from the NERC through grant NE/K006126.

The RESPONDER project is funded by a Consolidator Grant to Poul Christoffersen from the European Research Council, under the European Union's Horizon 2020 research and innovation programme.

Tom Chudley was supported by a Natural Environment Research Council Doctoral Training Partnership Studentship (Grant NE/L002507/1).

ArcticDEM was created from DigitalGlobe, Inc., imagery and funded under National Science Foundation awards 1043681, 1559691, and 1542736

SUPPLEMENTARY MATERIAL

Activity	Quantity	Unit
Energy consumption during measure and transmit	0.5	J
Duration of measure and transmit	3.2	s
Current consumption during sleep	500	nA
Nominal battery voltage	3.7	V
Power consumption during sleep	1.85	uW
Battery nominal voltage	3.7	V
Battery nominal capacity	400	mAh
Battery nominal capacity	1.48	Wh
Battery nominal capacity	5328	J
Derate factor for operating in the cold	50%	
Battery effective capacity in the field	2664	J
For 2 measurements per day:		
Active measurement time per day:	6.4	seconds
Sleep time per day	86393.6	seconds
Energy used whilst active	1	J
Energy used whilst asleep	0.16	J
Total energy used per day	1.16	J
Number of days the system will run for	2296	days
Number of years the system will run for	6.3	years

Table S1 – battery life calculation

REFERENCES

About LoRaWAN® | LoRa Alliance® https://lora-alliance.org/about-lorawan

Bagshaw EA, Burrow S, Wadham JL, Bowden J, Lishman B, Salter M, Barnes R and Nienow P (2012) E-tracers: Development of a low cost wireless technique for exploring sub-surface hydrological systems. *Hydrological Processes* **26**(20), 3157–3160 (doi:10.1002/hyp.9451)

Bagshaw E, Karlsson NB, Lishman B, Lok LB, Burrow S, Wadham JL, Clare L, Nicholls KW, Eisen O, Corr HFJ and Dahl-Jensen D (2018) Utilising Wireless Sensor Technologies in Glaciology. *AGU Fall Meeting Abstracts* **43** http://adsabs.harvard.edu/abs/2018AGUFM.C43D1823B

Bagshaw EA, Lishman B, Wadham JL, Bowden JA, Burrow SG, Clare LR and Chandler D (2014) Novel wireless sensors for in situ measurement of sub-ice hydrologic systems. *Annals of Glaciology* **55**(65), 41–50 (doi:10.3189/2014AoG65A007)

Barrella T, Barwick S and Saltzberg D (2011) Ross Ice Shelf in situ radio-frequency ice attenuation. *Journal of Glaciology* **57**(201), 61–66 (doi:10.3189/002214311795306691)

Barwick S, Besson D, Gorham P and Saltzberg D (2005) South Polar in situ radio-frequency ice attenuation. *Journal of Glaciology* **51**(173), 231–238 (doi:10.3189/172756505781829467)

Broeke MR van den, Enderlin EM, Howat IM, Kuipers Munneke P, Noël BPY, Berg WJ van de, Meijgaard E van and Wouters B (2016) On the recent contribution of the Greenland ice sheet to sea level change. *The Cryosphere* **10**(5), 1933–1946 (doi:https://doi.org/10.5194/tc-10-1933-2016)

Chandler DM, Wadham JL, Lis GP, Cowton T, Sole A, Bartholomew I, Telling J, Nienow P, Bagshaw EB, Mair D, Vinen S and Hubbard A (2013) Evolution of the subglacial drainage system beneath the Greenland Ice Sheet revealed by tracers. *Nature Geosci* **6**(3), 195–198 (doi:10.1038/ngeo1737)

Chu VW (2014) Greenland ice sheet hydrology: A review. *Progress in Physical Geography: Earth and Environment* **38**(1), 19–54 (doi:10.1177/0309133313507075)

Chudley TR, Christoffersen P, Doyle SH, Bougamont M, Schoonman CM, Hubbard B and James MR (2019) Supraglacial lake drainage at a fast-flowing Greenlandic outlet glacier. *PNAS* **116**(51), 25468–25477 (doi:10.1073/pnas.1913685116)

Church G, Bauder A, Grab M, Rabenstein L, Singh S and Maurer H (2019) Detecting and characterising an englacial conduit network within a temperate Swiss glacier using active seismic, ground penetrating radar and borehole analysis. *Annals of Glaciology* **60**(79), 193–205 (doi:10.1017/aog.2019.19)

Clarke GKC (1987) Subglacial till: A physical framework for its properties and processes. *Journal of Geophysical Research: Solid Earth* **92**(B9), 9023–9036 (doi:10.1029/JB092iB09p09023)

Doyle SH, Hubbard B, Christoffersen P, Young TJ, Hofstede C, Bougamont M, Box JE and Hubbard A (2018) Physical Conditions of Fast Glacier Flow: 1. Measurements From Boreholes Drilled to the Bed of Store Glacier, West Greenland. *Journal of Geophysical Research: Earth Surface* **123**(2), 324–348 (doi:10.1002/2017JF004529)

European Committee for Standardisation (2013) *BS EN 13757-4:2013 - Communication systems for meters and remote reading of meters . Wireless meter readout (Radio meter reading for operation in SRD bands).* https://bsol.bsigroup.com/en/Bsol-Item-Detail-Page/?pid=000000000030249978

Flowers GE (2018) Hydrology and the future of the Greenland Ice Sheet. *Nature Communications* **9**(1), 2729 (doi:10.1038/s41467-018-05002-0)

Friis HT (1946) A Note on a Simple Transmission Formula. *Proceedings of the IRE* **34**(5), 254–256 (doi:10.1109/JRPROC.1946.234568)

Griffiths J (1987) *Radio wave propagation and antennas.* Prentice-Hall

Gulley J (2009) Structural control of englacial conduits in the temperate Matanuska Glacier, Alaska, USA. *Journal of Glaciology* **55**(192), 681–690 (doi:10.3189/002214309789470860)

Hart JK, Martinez K, Basford PJ, Clayton AI, Robson BA and Young DS (2019) Surface melt driven summer diurnal and winter multi-day stick-slip motion and till sedimentology. *Nat Commun* **10**(1), 1–11 (doi:10.1038/s41467-019-09547-6)

Hoffman MJ, Andrews LC, Price SF, Catania GA, Neumann TA, Lüthi MP, Gulley J, Ryser C, Hawley RL and Morriss B (2016) Greenland subglacial drainage evolution regulated by weakly connected regions of the bed. *Nat Commun* **7**(1), 1–12 (doi:10.1038/ncomms13903)

Hofstede C, Christoffersen P, Hubbard B, Doyle SH, Young TJ, Diez A, Eisen O and Hubbard A (2018) Physical Conditions of Fast Glacier Flow: 2. Variable Extent of Anisotropic Ice and Soft Basal Sediment From Seismic Reflection Data Acquired on Store Glacier, West Greenland. *Journal of Geophysical Research: Earth Surface* **123**(2), 349–362 (doi:10.1002/2017JF004297)

Holmlund P and Hooke RLeb (1983) High Water-Pressure Events in Moulins, Storglaciären, Sweden. *Geografiska Annaler: Series A, Physical Geography* **65**(1–2), 19–25 (doi:10.1080/04353676.1983.11880070)

Hubbard BP, Sharp MJ, Willis IC, Nielsen MK and Smart CC (1995) Borehole water-level variations and the structure of the subglacial hydrological system of Haut Glacier d’Arolla, Valais, Switzerland. *Journal of Glaciology* **41**(139), 572–583 (doi:10.3189/S0022143000034894)

Iken A (1972) Measurements of Water Pressure in Moulins as Part of a Movement Study of the White Glacier, Axel Heiberg Island, Northwest Territories, Canada. *Journal of Glaciology* **11**(61), 53–58 (doi:10.3189/S0022143000022486)

Iken A (1981) The Effect of the Subglacial Water Pressure on the Sliding Velocity of a Glacier in an Idealized Numerical Model. *Journal of Glaciology* **27**(97), 407–421 (doi:10.3189/S0022143000011448)

Iken A and Bindschadler RA (1986) Combined measurements of Subglacial Water Pressure and Surface Velocity of Findelengletscher, Switzerland: Conclusions about Drainage System and Sliding Mechanism. *Journal of Glaciology* **32**(110), 101–119 (doi:10.3189/S0022143000006936)

Iken A, Echelmeyer K, Harrison W and Funk M (1993) Mechanisms of fast flow in Jakobshavns Isbræ, West Greenland: Part I. Measurements of temperature and water level in deep boreholes. *Journal of Glaciology* **39**(131), 15–25 (doi:10.3189/S0022143000015689)

Joughin I (2017) MEaSUREs Greenland Ice Velocity Annual Mosaics from SAR and Landsat, Version 1. (doi:10.5067/OBXCG75U7540)

Joughin I, Smith BE, Howat IM, Scambos T and Moon T (2010) Greenland flow variability from ice-sheet-wide velocity mapping. *Journal of Glaciology* **56**(197), 415–430 (doi:10.3189/002214310792447734)

Kamb B (1970) Sliding motion of glaciers: Theory and observation. *Reviews of Geophysics* **8**(4), 673–728 (doi:10.1029/RG008i004p00673)

Kamb B (1987) Glacier surge mechanism based on linked cavity configuration of the basal water conduit system. *Journal of Geophysical Research: Solid Earth* **92**(B9), 9083–9100 (doi:10.1029/JB092iB09p09083)

Karlsson NB and Dahl-Jensen D (2015) Response of the large-scale subglacial drainage system of Northeast Greenland to surface elevation changes. *The Cryosphere* **9**(4), 1465–1479 (doi:https://doi.org/10.5194/tc-9-1465-2015)

Lewis C, Gogineni S, Rodriguez-Morales F, Panzer B, Stumpf T, Paden J and Leuschen C (2015) Airborne fine-resolution UHF radar: an approach to the study of englacial reflections, firn compaction and ice attenuation rates. *J. Glaciol.* **61**(225), 89–100 (doi:10.3189/2015JoG14J089)

Martinez K, Basford PJ, Jager DD and Hart JK (2013) Using a heterogeneous sensor network to monitor glacial movement. 2

Martinez K, Ong R and Hart J (2004) Glacsweb: a sensor network for hostile environments. *2004 First Annual IEEE Communications Society Conference on Sensor and Ad Hoc Communications and Networks, 2004. IEEE SECON 2004.* 81–87 (doi:10.1109/SAHCN.2004.1381905)

Moore RD (2005) Introduction to salt dilution gauging for streamflow measurement Part 3: Slug injection using salt in solution. *Streamline Watershed Management Bulletin* **8**(2), 1–6

Morlighem M, Williams CN, Rignot E, An L, Arndt JE, Bamber JL, Catania G, Chauché N, Dowdeswell JA, Dorschel B, Fenty I, Hogan K, Howat I, Hubbard A, Jakobsson M, Jordan TM, Kjeldsen KK, Millan R, Mayer L, Mouginot J, Noël BPY, O'Cofaigh C, Palmer S, Rysgaard S, Seroussi H, Siegert MJ, Slabon P, Straneo F, van den Broeke MR, Weinrebe W, Wood M and Zinglersen KB (2017) BedMachine v3: Complete Bed Topography and Ocean Bathymetry Mapping of Greenland From Multibeam Echo Sounding Combined With Mass Conservation. *Geophysical Research Letters* **44**(21), 11,051-11,061 (doi:10.1002/2017GL074954)

Ng FSL (2000) Canals under sediment-based ice sheets. *Annals of Glaciology* **30**, 146–152 (doi:10.3189/172756400781820633)

Nienow PW, Hubbard AL, Hubbard BP, Chandler DM, Mair DWF, Sharp MJ and Willis IC (2005) Hydrological controls on diurnal ice flow variability in valley glaciers. *Journal of Geophysical Research: Earth Surface* **110**(F4) (doi:10.1029/2003JF000112)

Nienow PW, Sole AJ, Slater DA and Cowton TR (2017) Recent Advances in Our Understanding of the Role of Meltwater in the Greenland Ice Sheet System. *Curr Clim Change Rep* **3**(4), 330–344 (doi:10.1007/s40641-017-0083-9)

Nye JF (1976) Water Flow in Glaciers: Jökulhlaups, Tunnels and Veins. *Journal of Glaciology* **17**(76), 181–207 (doi:10.3189/S002214300001354X)

Plewes LA and Hubbard B (2016) A review of the use of radio-echo sounding in glaciology: *Progress in Physical Geography* (doi:10.1177/030913330102500203)

Porter C, Morin P, Howat I, Noh M-J, Bates B, Peterman K, Keesey S, Schlenk M, Gardiner J, Tomko K, Willis M, Kelleher C, Cloutier M, Husby E, Foga S, Nakamura H, Platson M, Wethington M Jr, Williamson C, Bauer G, Enos J, Arnold G, Kramer W, Becker P, Doshi A, D'Souza C, Cummens P, Laurier F and Bojesen M (2018) ArcticDEM. (doi:10.7910/DVN/OHHUKH)

Pritchard HD, Arthern RJ, Vaughan DG and Edwards LA (2009) Extensive dynamic thinning on the margins of the Greenland and Antarctic ice sheets. *Nature* **461**(7266), 971–975 (doi:10.1038/nature08471)

RC1701xx-MBUS Datasheet (2018) https://radiocrafts.com/uploads/rc1701xx-mbus_datasheet.pdf

Röthlisberger H (1972) Water Pressure in Intra- and Subglacial Channels *. *Journal of Glaciology* **11**(62), 177–203 (doi:10.3189/S0022143000022188)

Röthlisberger H (1980) Gletscherbewegung und Wasserabfluss. *Wasser*, *Energie*, *Luft* **72**(9), 290–294

Röthlisberger H and Lang H (1987) Glacial Hydrology. *Glacio-Fluvial Sediment Transfer: An Alpine Perspective*. Wiley, 207–84

Schoof C (2010) Ice-sheet acceleration driven by melt supply variability. *Nature* **468**(7325), 803–806 (doi:10.1038/nature09618)

Sheldon SG, Steffensen JP, Hansen SB, Popp TJ and Johnsen SJ (2014) The investigation and experience of using ESTISOL^{TM} 240 and COASOL^{TM} for ice-core drilling. *Annals of Glaciology* **55**(68), 219–232 (doi:10.3189/2014AoG68A036)

Smeets CJPP, Boot W, Hubbard A, Pettersson R, Wilhelms F, Broeke MRVD and Wal RSWVD (2012) A wireless subglacial probe for deep ice applications. *Journal of Glaciology* **58**(211), 841–848 (doi:10.3189/2012JoG11J130)

Sole AJ, Mair DWF, Nienow PW, Bartholomew ID, King MA, Burke MJ and Joughin I (2011) Seasonal speedup of a Greenland marine-terminating outlet glacier forced by surface melt–induced changes in subglacial hydrology. *Journal of Geophysical Research: Earth Surface* **116**(F3) (doi:10.1029/2010JF001948)

Tedstone AJ, Nienow PW, Gourmelen N, Dehecq A, Goldberg D and Hanna E (2015) Decadal slowdown of a land-terminating sector of the Greenland Ice Sheet despite warming. *Nature* **526**(7575), 692–695 (doi:10.1038/nature15722)

Tranter M, Sharp MJ, Lamb HR, Brown GH, Hubbard BP and Willis IC (2002) Geochemical weathering at the bed of Haut Glacier d'Arolla, Switzerland—a new model. *Hydrological Processes* **16**(5), 959–993 (doi:10.1002/hyp.309)

UM10204 I2C-bus specification and user manual (2014) **2014**, 64

Vallelonga P, Christianson K, Alley RB, Anandakrishnan S, Christian JEM, Dahl-Jensen D, Gkinis V, Holme C, Jacobel RW, Karlsson NB, Keisling BA, Kipfstuhl S, Kjær HA, Kristensen MEL, Muto A, Peters LE, Popp T, Riverman KL, Svensson AM, Tibuleac C, Vinther BM, Weng Y and Winstrup M (2014) Initial results from geophysical surveys and shallow coring of the Northeast Greenland Ice Stream (NEGIS). *The Cryosphere* **8**(4), 1275–1287 (doi:10.5194/tc-8-1275-2014)

Walder JS (1986) Hydraulics of Subglacial Cavities. *Journal of Glaciology* **32**(112), 439–445 (doi:10.3189/S0022143000012156)

Werder MA, Schuler TV and Funk M (2010) Short term variations of tracer transit speed on alpine glaciers. *The Cryosphere* **4**(3), 381–396 (doi:https://doi.org/10.5194/tc-4-381-2010)

Young TJ, Schroeder DM, Christoffersen P, Lok LB, Nicholls KW, Brennan PV, Doyle SH, Hubbard B and Hubbard A (2018) Resolving the internal and basal geometry of ice masses using imaging phase-sensitive radar. *Journal of Glaciology* **64**(246), 649–660 (doi:10.1017/jog.2018.54)